J. Fluid Mech. (1969), *vol.* 36, *part* 1, *pp.* 21–31
Printed in Great Britain

Experiments on natural convection in enclosures with localized heating from below

By K. E. TORRANCE, L. ORLOFF AND J. A. ROCKETT
National Bureau of Standards, Washington, D.C., 20234

(Received 24 June 1968)

An experimental study was made of the steady-state natural convection induced in enclosures by a small hot spot centrally located on the floor. Enclosures of rectangular and circular floor plan were employed, with height equal to one-half the major dimension of the floor plan. The movement of air within the chambers was made visible by adding metaldehyde dust particles and illuminating them with an intense light beam. The Grashof number (Gr) based on hot-spot temperature and enclosure height ranged from 8×10^5 to 1×10^{10}. Laminar flows were observed for $Gr \lesssim 1{\cdot}2 \times 10^9$. The experimental flows in the circular chamber are compared in a companion paper with theoretically calculated flows (Torrance & Rockett 1969). In the region of laminar flows the agreement was excellent. The present paper notes certain similarities in the flows in rectangular and circular geometries. The disturbing effect of a slight heating of one wall of the rectangular enclosure was also investigated. Measurements were made of heat transfer from the hot spot to the air in the chamber.

1. Introduction

The earliest possible detection of a building fire is of paramount importance to both the safety of the occupants and property conservation. Most fire detectors depend on natural convection to carry evidence of the fire to the detector. This gas convection is part of the general natural convective flow induced by an incipient fire. The detector itself may sense heat, ions, smoke, carbon monoxide or almost anything else that can be detected in abnormal quantities and which can be reliably associated with the presence of a fire. It follows that the design of an efficient fire detection and localization system requires a knowledge of the natural convection currents likely to arise in the event of a fire. A full understanding of these flows represents a formidable task because of the complexity of the basic fire phenomenon and because many parameters are involved, such as the size and location of the fire, building geometry, and so on. We simplify the problem by substituting a small heat source for the fire, and then look at the natural convection flows arising in a closed model room when this small heat source is placed on the floor.

Several investigators have looked at the air flow into a fire and the convection plume above it (Taylor 1961, Lee & Emmons 1961 and Thomas, Baldwin & Heselden 1965). Still others have examined the convective air flow associated

with a fire in rather specialized geometries (Thomas 1961). The present authors know of no prior studies of air movement in closed spaces under incipient fire conditions or even with an equivalent heat source so situated as to simulate fire conditions. It was to provide information of this type that the present study was undertaken.

This study reports a systematic experimental investigation of the steady-state natural convective air motion arising in small unfurnished chambers from a localized heat source on the floor. Chambers of various sizes with rectangular and circular floor plans were employed. A technique was devised whereby very light, highly reflective particles of metaldehyde (polymerized acetaldehyde) were added to the chambers. A sheet of intense light was passed through the chamber and the particle streaks, or flow patterns, were photographed. By varying the size of the enclosure and the heat source temperature, a wide range of Grashof numbers (Gr) was covered. This parameter is defined as

$$Gr = \frac{g\beta\Delta T a^3}{\nu^2}, \tag{1}$$

where a is the height of the chamber and g is the acceleration of gravity. The thermal driving force is the temperature difference $\Delta T = T_h - T_0$, where T_h and T_0 are the uniform temperatures of the heat source and surrounding cold walls respectively. The volume expansion coefficient and kinematic viscosity of air are respectively denoted by β and ν, and are evaluated at the temperature T_0. Both laminar and turbulent flows were observed experimentally, the laminar flows receiving the greater attention. This was because the laminar flows could be compared with the theoretical flows presented in a companion paper (Torrance & Rockett 1969). For the test chambers with circular floor plan, the height was equal to the radius, while the rectangular chambers of height a utilized a floor plan $2a$ by a. In all cases, the heat source on the floor was a uniform-temperature disk with a radius of about one-tenth the enclosure height.

Details of the experiment and the test chambers are discussed in § 2, followed by results in § 3.

2. Experimental

An experimental apparatus was set up to permit us to visualize and photograph natural convection flow patterns in enclosures. The technique used centred around the conventional light beam/dust particle method. A schematic diagram of the apparatus is shown in figure 1, which illustrates a cylindrical enclosure E of height a and radius b resting upon a floor F. For the case of a rectangular enclosure, b would be the half-width of the chamber. The enclosure walls are at a temperature T_0, except for a small centrally located disk G on the floor of radius c, which is held at a temperature $T_h > T_0$. The temperature driving force $\Delta T = T_h - T_0$ initiates and sustains the natural convective motion within the chamber. Air is used as the working fluid, to which special dust particles are added. A light source and optics (A, B, C and D) provide an intense, narrow beam of light which passes through the transparent vertical walls of the chamber, thus illuminating the dust particles. The motion of the particles is recorded by a

camera, the axis of which is perpendicular to the plane of illumination. The entire apparatus is supported by thermal insulating material H and I. The ×-symbols denote thermocouple locations. A detailed description of the experimental apparatus and procedure will now be presented. Readers wishing to examine the results directly may proceed to §3.

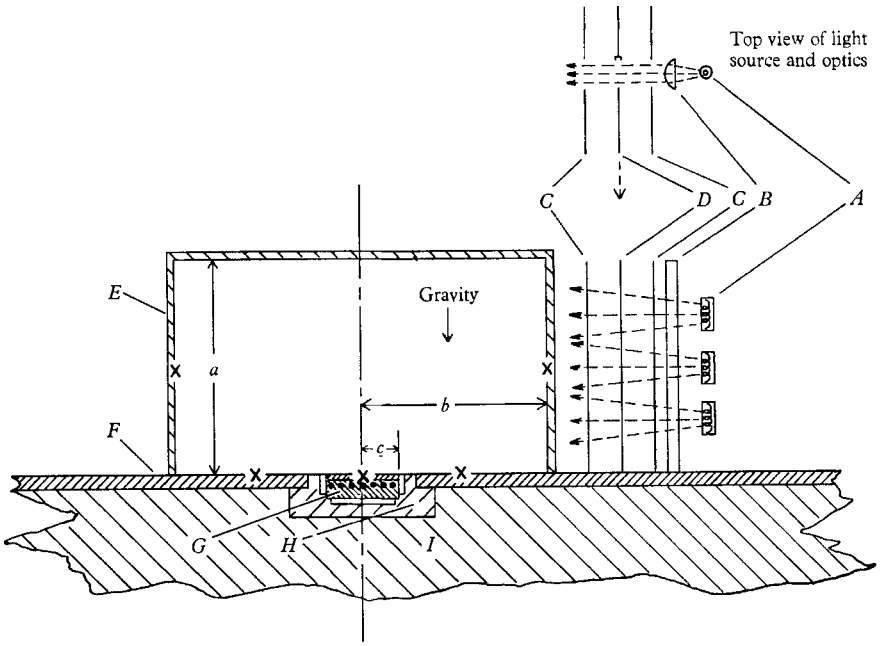

FIGURE 1. Schematic diagram of experimental apparatus.

Various chambers were used in this study. A small rectangular chamber of 6·4 mm acrylic plastic with 15·2 × 30·5 cm floor plan and 15·2 cm height was used for checking out the apparatus and for surveying the flow patterns as we systematically varied the experimental conditions: the thermal driving force ΔT, location of the heated disk relative to the walls, and the combination of a centrally located heated disk and a superimposed heating of one wall. A sequence of circular cylindrical chambers with height equal to radius was employed expressly to provide data for comparison with calculated flows developed in a companion paper by assuming radial symmetry. These chambers were designed to cover a wide range of Grashof numbers which would extend into the turbulent régime. Chambers of height (or radius) 9·5, 14·9 and 45·4 cm were utilized. The smallest chamber used 6·4 mm acrylic plastic walls and a 3·2 mm thick copper ceiling, the middle chamber used 3·2 and 6·4 mm acrylic plastic for the walls and ceiling, respectively. In order to maintain the walls of the largest chamber at a nearly uniform temperature, the walls and ceiling were constructed of 3·2 mm aluminium. A 1·6 mm acrylic plastic lining was attached to the inside of the vertical walls. Doors were installed in the aluminium walls to permit passage of the light beam and camera viewing.

The floor F (see figure 1) of the test chambers consisted of large sheets of either

3·2 mm copper or 6·4 mm aluminium. In the centre of the floor, an asbestos millboard insulating ring H held the electrically heated disk G. For additional thermal insulation, a small air gap was provided between the ring and the disk, as shown. The floor and insulating ring were supported by rigid polyurethane foam insulation I. The heater G consisted of two pieces: a metal top disk fastened to an aluminium silicate bottom disk. The lower disk held the nichrome heater element. The metal top disk was used to achieve a nearly uniform surface temperature; these disks were of either chrome-plated copper or polished stainless steel, for use at low or high temperatures respectively. The radius c of the various heaters used was 0·64 cm for the small round chamber, 1·00 cm for the rectangular and medium round chambers, and 3·33 cm for the large round chamber. The first two heaters were 0·4 cm thick and the latter was 1·5 cm thick. The radius of the hole in the floor F for the three heaters was, respectively, 1·1, 1·7 and 5·7 cm. The heater disk radii approximate one-tenth of the chamber height, which was the heater size used in the theoretical companion paper. A survey of radial floor temperature profiles revealed that, outside the air gap and insulating ring H, the floor temperature was not sufficiently high to cause preheating of the air as it approached the hot disk G. There was, however, a measurable radial heat loss from the disk to the floor, F, which is discussed in a later paragraph.

The light source A consisted of three 500 W tungsten iodide lamps. For the smallest chamber, a single 1000 W carbon arc was substituted. The light from either of these sources passed through a cylindrical condensing lens B and a pair of narrow vertical collimating slits C. These slits were adjusted so that the width of the light beam was about one-half the heater disk diameter. This light beam also passed through 5 cm of acrylic plastic (not shown in figure 1) which absorbed most of the infrared. Without this, the acrylic plastic chamber walls would have absorbed the heat, causing troublesome local hot spots on the wall where the beam entered and left the chamber. Also in the source optics was an electromechanical slit shutter D which was actuated by the time base of an oscilloscope. The shutter was normally closed to minimize heating by the beam. The light source and optics could be moved as a unit to vary the place where the light beam passed through the chamber. For most of the study, and for all of the results presented here, this section was taken through the centre of the disk heater. A 10·2 × 12·7 cm plate camera with an $f/3{\cdot}5$ lens of 12 cm focal length was employed. The focal plane of the camera was parallel to the light beam. High-speed film (ASA 3000) was used. During the film exposures, the camera lens was open and the light beam shutter was used to time the exposure.

For data-taking, an insulated hood was placed over the test chamber and camera. Narrow slits permitted the light beam to enter and leave. This hood helped to isolate the chamber from extraneous heat sources in the laboratory. Without this, all manner of trouble was experienced from apparently insignificant heat sources around the room, such as vacuum tubes, autotransformers, the operator, etc. This problem was evident as a disturbance of the flow patterns, causing presumably symmetric flows to be non-symmetric.

Thermocouples of 0·32 mm diameter chromel–alumel wire were placed on the floor, on the heated disk, and on the walls, as indicated by the ×-symbols in

figure 1. Thermocouples on opposing pairs of walls were read differentially with a null microvoltmeter. Other thermocouples were read with a microvolt potentiometer. The temperature T_h of the heated disk was measured with a surface thermocouple. The wall temperature T_0 was obtained by averaging the temperature of the enclosure walls and floor. It was necessary to maintain the temperature difference between opposing pairs of walls to less than 0·03 degC if spurious effects on the flow were to be avoided at the lower Grashof numbers. For this reason, high thermal conductivity metal was used in the fabrication of some of the chambers when feasible. The temperature of the enclosure walls could usually be brought within the prescribed tolerance by allowing the chamber, heater disk, and insulated hood to stand undisturbed for several hours before attempting a photograph.

Numerous additives were used to render the flow visible. Early success was achieved with the spores of the puffball mushroom. The spores were a dark brown after drying and had to be dispensed directly from the mushroom in order to avoid clumping into large, heavy masses. A much more satisfactory material, known as metaldehyde (polymerized acetaldehyde) was suggested by Daws, Penwarden & Waters (1965) and apparently first by Schmieschek (1936). This material comes as a white crystalline solid, which sublimes readily when heated with a hot nichrome coil. It almost immediately condenses back to the solid phase to form lightweight, filamentary particles somewhat like miniature dandelion seeds. These particles are white in colour and very reflective, and were used throughout the data-taking part of this programme. The particles were introduced into the chamber through a trapdoor in the floor, and initially had a large range of sizes. The large ones were allowed to settle out leaving those less than about 1 mm in diameter floating in the air. These have such a small settling rate that it can be assumed that they follow the air movement closely. To reduce the accumulation of particles on the plastic chamber walls, the walls were sprayed with anti-static liquid. Metaldehyde is also used as a solid fuel by alpinists and as an agricultural pesticide; thus it is readily obtained commercially. Ingestion of the solid or prolonged breathing of the vapour is not recommended.

For the series of tests in which the disk on the floor and one wall were simultaneously heated, the 15·2 × 15·2 × 30·5 cm rectangular chamber was used. One 15·2 × 15·2 cm wall was uniformly heated electrically with a mesh of fine nichrome wire. The heating rate was determined by measuring the voltage and current. Thermocouples were used to sense the heated wall temperature, which varied slightly over the surface. For several fixed heating rates of the wall, the heater disk temperature was varied. Results for a wall heating rate of about 0·01 W/cm^2 are presented in §3.3 of this report. For ease of comparison, the amount of wall heating is expressed in terms of temperature difference, which was about 5 degC, between the centre of the heated wall and the centre of the opposite wall.

An auxiliary determination of heat transfer from the heated disk to the air in the enclosure was also made. This entailed measurement of the electric power supplied to the disk with a precision wattmeter and then subtracting any heat losses. For these tests, the metal surface of the disk was gold plated. This made radiation losses negligible, so that the only heat loss of significance was by

conduction through the supporting insulation. A temperature survey of this region revealed that most of this heat loss found its way to the highly conductive metal floor. Very careful measurements of the temperature drop along a radius of the floor, together with the known thermal conductivity of the floor, established the magnitude of this loss. The conduction loss was 65% for the single, lowest Grashof number point. For the remaining points this loss ranged from 40 to 15%, with the larger percentage at lower Grashof numbers.

3. Results

Photographs of steady-state flow patterns for a range of experimental conditions are presented in figures 2–5. Of these, figures 2 and 3 illustrate the effect of varying the Grashof number in the rectangular enclosure with a centrally located hot spot, whereas figure 4 illustrates the same effect for the various circular cylindrical chambers. The effect of superimposing a slight heating of one wall of the rectangular enclosure is shown in figure 5 for a range of heating disk temperatures. An exposure time of two seconds was used for all photographs except figures 3 and 4(*e*), for which an exposure time of five seconds was used. The pictures shown are representative of a much larger body of data actually obtained.

3.1. *The rectangular chamber*

Figure 2, plate 1, illustrates the effect of raising the temperature of the heated disk, or the Grashof number, with the disk in the centre of the floor. The light beam passes through the chamber in the long direction, so that the illuminated plane is 15·2 × 30·5 cm. Wall thermocouples are visible on the left and right sides, as are some reflexions on the ceiling and walls. The bright object on the ceiling to the left of the rising column is a particle insertion port for the mushroom spores used early in the programme. Metaldehyde particles were used for the present photographs, and were introduced through a trapdoor in the floor (not visible in the photographs). The ability of the metaldehyde particles to follow the flows accurately is evident in figure 2. Only a few heavy particles appear to be settling out, as shown by the bright streaks crossing other particle paths in figures 2(*c*) and (*d*).

Figures 2(*a*)–(*d*) respectively apply to heating disk temperatures above ambient (ΔT) of 8, 16, 77 and 292 degC, or alternately, Grashof numbers (Gr) of 4×10^6, 8×10^6, 4×10^7 and $1{\cdot}4 \times 10^8$. The flow patterns are generally similar, with a column of heated air rising above the hot spot and impacting the ceiling. The impact forms a wall jet along the ceiling which spreads out radially and turns downward when it reaches the vertical wall. The air then turns inward and moves toward the centre to be again entrained in the rising column. During the course of this circulation, the particle paths describe a vortex motion, the centre of which is evident on both sides of the column. As the hot-spot temperature is raised, these symmetrically located vortex centres are flattened against the ceiling and elongated. The flow patterns are all quite symmetrical, even for the very weak flow shown in figure 2(*a*) with a ΔT of only 8 degC. This symmetry is to be expected for a geometrically centred hot spot. However, as will be shown in

§3.3, a very slight heating of one of the vertical walls would render the flow unsymmetric. The observed symmetry is a result of following the experimental precautions detailed earlier. The highest temperatures achievable with the electrically heated spot were not sufficient to produce turbulence in this chamber.

The flow patterns observed when the light beam sections the chamber at right angles to the orientation of figure 2 are shown in figure 3, plate 2, where the illuminated plane is $15{\cdot}2 \times 15{\cdot}2$ cm. Figures 3 (*a*) and (*b*) respectively pertain to $\Delta T = 52$ degC ($Gr = 3 \times 10^7$) and $\Delta T = 290$ degC ($Gr = 1{\cdot}4 \times 10^8$). Many heavy particles can be seen settling out in both photographs. The difference between the two flows is striking, and is attributed to three-dimensional effects which became apparent in this plane for $\Delta T \gtrsim 60$ degC. For ΔT less than this value, the flow patterns along the two axes of the 2:1:1 rectangular chamber were very similar, the one simply appearing as a stretched version of the other. For $\Delta T \gtrsim 60$ degC, this similarity disappeared, due to the appearance of 'sources' and 'sinks' in the plane along the short axis. There are, of course, no true sources or sinks, only three-dimensional flow movement. The strength of these effects increased with increasing ΔT. The flow in figure 3 (*b*) is typical, with streak patterns suggestive of sources appearing in the lower left- and right-hand regions where fluid moves into the plane of illumination.

Two additional studies were made to explore general flow patterns. In one, the hot spot was moved relative to the walls (by moving the chamber on the base plate); in the other, the light beam was moved relative to the hot spot. It was found that the flow patterns were little affected by the walls (provided they were at a uniform temperature) until the rising column was within a few heating-disk diameters of a wall. Also, it was found that the flow patterns away from the symmetry plane were little different from those to be expected in a cylindrical chamber with the hot spot on the axis (for heating disk $\Delta T \lesssim 60$ degC). These two observations are self-consistent and are consistent with the intuitive idea that, due to the requirement of continuity, the flow is rapid only inside or near the boundary of the rising column. With increasing radial distance from the column the velocities must rapidly decrease. Placing an obstruction in the low-velocity region will affect that region, but will not significantly alter the column. It was, in part, due to this observation that the parallel analytical work was undertaken in cylindrically symmetric co-ordinates.

3.2. *The circular cylindrical chambers*

The purpose of this programme was to obtain data suitable for direct comparison with numerical solutions of the equations of motion in cylindrical co-ordinates. Accordingly, the flow patterns shown in figure 4 (*a*)–(*e*), plates 3–4, were obtained, respectively, at Grashof numbers of 8×10^5, 4×10^6, 4×10^7, 3×10^8 and 1×10^{10}. The heated disk is centrally located and the light beam crosses the chamber along a diameter. The wide range of Gr was achieved by varying both enclosure size and the thermal driving force ΔT. Figure 4 (*a*) and (*b*) were obtained in the 9·5 cm high chamber with $\Delta T = 7{\cdot}1$ and 31·6 degC respectively; figure 4 (*c*) and (*d*) were obtained in the 14·9 cm high chamber with $\Delta T = 81$ and 635 degC respectively; figure 4 (*e*) was obtained in the 45·4 cm high chamber with $\Delta T = 752$ degC.

The flow patterns in the laminar region (figure 4(*a*)–(*d*)) display a variation with Gr and a general appearance which is very similar to that found in the rectangular chamber (figure 2). In this connexion, figure 4(*b*), (*c*) and (*d*) may be directly compared with figure 2(*a*), (*c*) and (*d*). This offers additional support for the choice of a cylindrical geometry for further study.

For Grashof numbers above about $1{\cdot}2 \times 10^9$, turbulence was observed. Considerable effort was made to obtain a photograph at $Gr = 1 \times 10^9$ in the 45·4 cm high chamber and in another chamber 31 cm high. Due to the sensitive nature of the flow so close to the onset of transition, a picture could not be obtained of a quality comparable to the others in this report. The first visual appearance of turbulence just above $Gr = 1{\cdot}2 \times 10^9$ was in the form of small eddies which originated at the edge of the rising column as it impacted the ceiling. These eddies rolled out along the ceiling and turned downward with the general flow near the outer wall. By this time, they had diffused much of their strength, and they soon disappeared in the general flow of air returning to the rising column. These turbulent eddies appeared almost periodically, at intervals of a few seconds. As Gr was increased still further, the scale and number of turbulent eddies increased, but the turbulence generally remained near the ceiling. Figure 4(*e*) illustrates a predominantly turbulent flow at $Gr = 1 \times 10^{10}$. Only the flow near the floor is laminar. As fluid approaches the edge of the rising column, it undergoes a transition to turbulence. This transition is characterized by an oscillatory motion of increasing amplitude, sometimes taking on a corkscrew-like appearance.

The laminar flow patterns in figure 4(*a*)–(*d*) are compared with calculated streamlines in the companion paper, Torrance & Rockett (1969). Good agreement is found to exist. This is true even though the ΔT used in figure 4(*d*) was so large as to violate the Boussinesq approximation used for the theory. When extended into the turbulent range, the calculated flows developed a periodic vortex shedding at $Gr = 4 \times 10^{10}$, suggestive of the eddies described above at the onset of transition.

A few additional details in figure 4 may be noted. The flow at $Gr = 8 \times 10^5$ (figure 4(*a*)) is not quite symmetric. The wall temperature was monitored at four locations on the perimeter. The left side of the chamber was less than 0·01 degC warmer than the other points sampled when the photograph was taken. This was the best picture that could be achieved for this very weak flow condition. At higher Gr, figure 4(*c*)–(*e*), the settling of a few heavy particles shows up as bright streaks crossing fainter streaks of lighter particles. At these Gr, large flow velocities are found only in the rising column and the wall jet boundary layer near the solid walls. Elsewhere, relatively slow motion exists. Heavy particles in this slow, central region tend to settle under the influence of gravity, but as they near the floor they are swept back into the flow. Thus, they do not actually settle to the floor, as they did in figure 4(*a*) and (*b*) (and also figures 2(*a*) and (*b*)). Also, at higher hot-spot temperatures, ΔT, the metaldehyde particles near the hot spot vaporize, with the result that no particles appear along the centreline.

3.3. *The rectangular chamber with a superimposed heating of one wall*

Several times in the foregoing, we mentioned that a slight heating of the wall had a very disturbing effect on the flow in the chambers. This effect is illustrated in figure 5, plate 5, for the rectangular chamber with the heating disk centrally located on the floor. The light beam illuminates a 15·2 cm by 30·5 cm section through the centre of the hot spot. The right-hand wall (15·2 × 15·2 cm) is held at a temperature 5 degC above the remaining five faces of the chamber while the temperature of the heated disk is varied. Figures 5(*a*)–(*d*) respectively apply to heating disk temperatures relative to ambient (ΔT) of 0, 8, 20 and 300 degC. The corresponding Grashof numbers based on this ΔT are 0, 4×10^6, 1×10^7 and $1{\cdot}5 \times 10^8$ respectively.

Figure 5(*a*) illustrates the flow arising from the heated wall when the disk on the floor is unheated. The flow is not symmetrical because the wall heating is not symmetrical. For symmetry, the left wall should be simultaneously cooled 5 degC below ambient. The air flows upward along the right wall. Just below the ceiling is a region of rapid flow to the left. Below this is an elongated vortex core and then an extensive region of slow flow to the right. Near the bottom, particles can be seen settling to the floor.

The basic flow of figure 5(*a*) is combined with the flows from the heated disk shown in figures 2(*a*), (*b*) and (*d*), to give the flow patterns shown in figures 5(*b*), (*c*) and (*d*) respectively. Figure 5(*b*) portrays the effect of a weak hot spot, when the rising column is washed away by the general left-to-right flow. Figure 5(*c*) shows the result of more vigorous heating of the disk. The rising column does not, however, impinge on the ceiling. There is a layer of air from the heated right wall flowing from right to left between the stagnation point at the top of the column and the ceiling. Figure 5(*d*) shows that, with sufficiently vigorous heating of the disk on the floor, the column can break through to the ceiling. In this picture, the general room circulation from the heated wall has divided and flows around the column.

Disk radius 1·00 cm		Disk radius 3·33 cm	
$\Delta T = T_h - T_0$ (degC)	$\dot{Q}$ (W)	$\Delta T = T_h - T_0$ (degC)	$\dot{Q}$ (W)
16	0·04	73	3·0
89	0·4	170	7·8
146	0·7	280	18
165	0·9	300	20
205	1·1	372	25
		512	41
		636	70

TABLE 1. Heat transfer $\dot{Q}$ by natural convection from a heated disk in a floor to air above

3.4. *Heat transfer rates*

The rate of heat transfer from the disk in the floor to the air in the enclosure was determined for a range of Grashof numbers. The results are presented in table 1

as a rate of heat transfer $\dot{Q}$ (in watts) for disks 1·00 and 3·33 cm in radius at various temperatures ΔT. The heat transfer rates are believed to be accurate to 20% at the lower values of $\dot{Q}$ and to 10% at the higher values. Temperatures are rounded to the nearest degree. These results are put in dimensionless form and compared with theory in figure 9 of the companion paper.

4. Conclusions

An experimental technique was developed which permitted systematic study of laminar flows induced by a simulated fire. The axisymmetric flows in a cylindrical chamber were thoroughly documented from creeping flow to turbulence. This part of the programme was done in support of a parallel analytic study. Similar work to delineate the effect of varying chamber aspect ratio is indicated and is in progress.

The experimental study of rectangular chambers has not been complemented by an analytic investigation. The general features of the flows in this geometry are not too surprising in retrospect. The relative insensitivity of the column to the presence of unsymmetrically placed walls and its great sensitivity to quite weak background convection is of interest. The nature of the three-dimensional flow introduced at the higher Grashof numbers in the rectangular chamber was not anticipated. The complexity of the flows in this very simple geometry suggests the danger of moving too rapidly to 'more realistic' configurations.

The use of laminar flow experiments to simulate what is assuredly turbulent in the ultimate application requires care. The time-average fluid motion does not change qualitatively, in our apparatus, with the transition to turbulence. This suggests the possibility of using laminar flows to predict mean turbulent motion by using a suitably adjusted viscosity. Such a prediction is premature, at present, but merits further research. Our original purpose, to be able to make meaningful statements about the optimal placing of fire detectors, must await the results of this research.

The authors would like to thank Professor Howard W. Emmons of Harvard University for many helpful discussions during the course of this work. This paper is a contribution of the National Bureau of Standards and is not subject to copyright.

REFERENCES

Daws, L. F., Penwarden, A. D. & Waters, G. T. 1965 A visualization technique for the study of air movement in rooms. *J. Instn. Heat. Vent. Engs.* **33**, 24.

Lee, S-L. & Emmons, H. W. 1961 A study of natural convection above a line fire. *J. Fluid Mech.* **11**, 353.

Schmieschek, U. 1936 Sichtbarmachung und Messung von Luftströmungen. *Z. tech. Phys.* **17**, 98.

Taylor, G. I. 1961 Fire under influence of natural convection. International Symposium on *The Use of Models in Fire Research*, Publication 786, National Academy of Sciences —National Research Council (Washington, D.C.), 10.

THOMAS, P. H. 1961 Some studies of building fires using models. International Symposium on *The Use of Models in Fire Research*, Publication 786, National Academy of Sciences—National Research Council (Washington, D.C.), 150.

THOMAS, P. H., BALDWIN, R. & HESELDEN, A. J. M. 1965 Buoyant diffusion flames: some measurements of air entrainment, heat transfer, and flame merging; *Tenth Symposium (International) on Combustion*, The Combustion Institute, 983.

TORRANCE, K. E. & ROCKETT, J. A. 1969 Numerical study of natural convection in an enclosure with localized heating from below—creeping flow to the onset of laminar instability. *J. Fluid Mech.* **36**, 33.

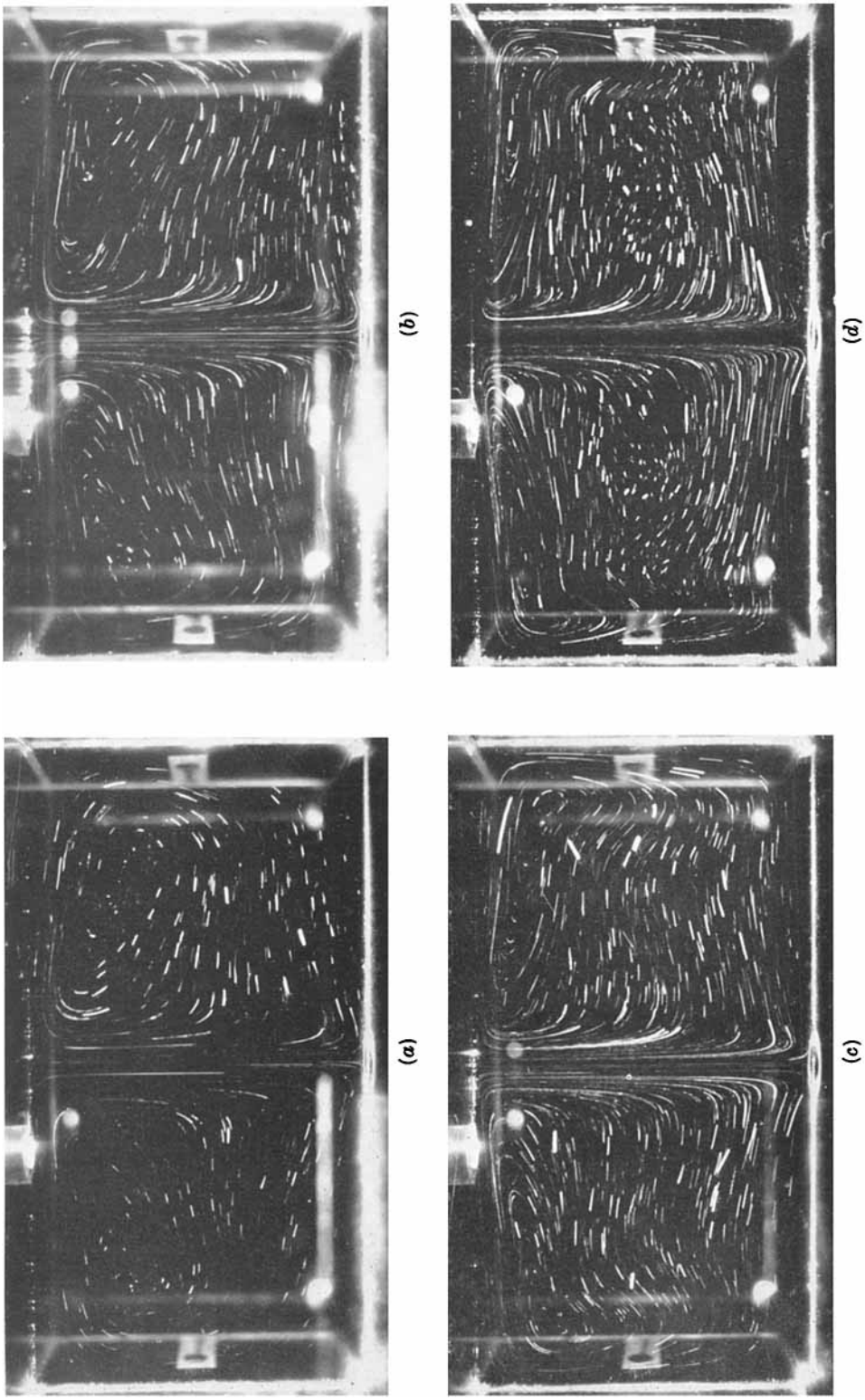

FIGURE 2. Effect of varying the Grashof number (Gr) in the rectangular enclosure. Illumination through the centre of the heated disk parallel to the longer walls. (*a*) $Gr = 4 \times 10^6$; (*b*) $Gr = 8 \times 10^6$; (*c*) $Gr = 4 \times 10^7$; (*d*) $Gr = 1{\cdot}4 \times 10^8$.

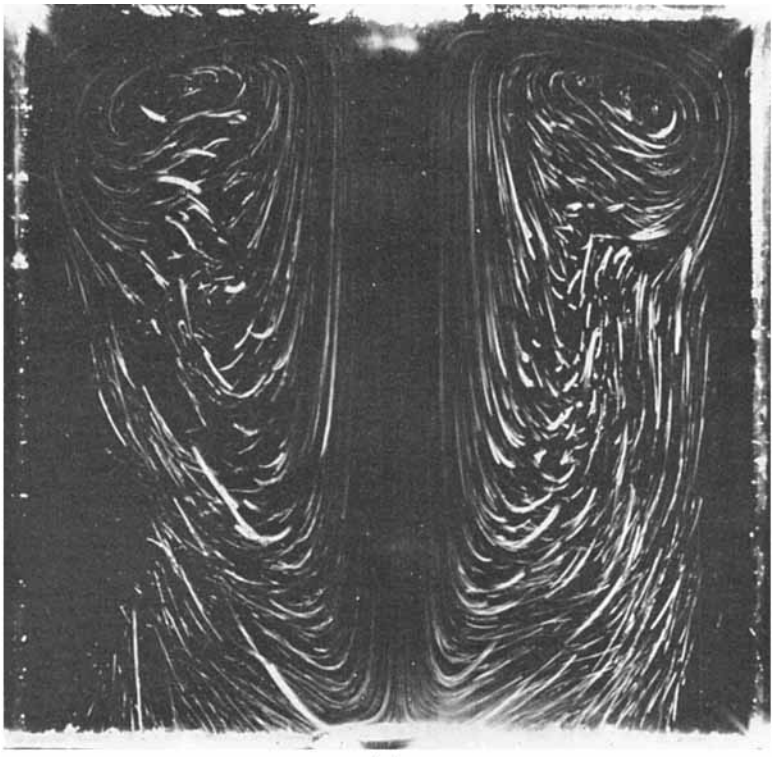

(*a*)

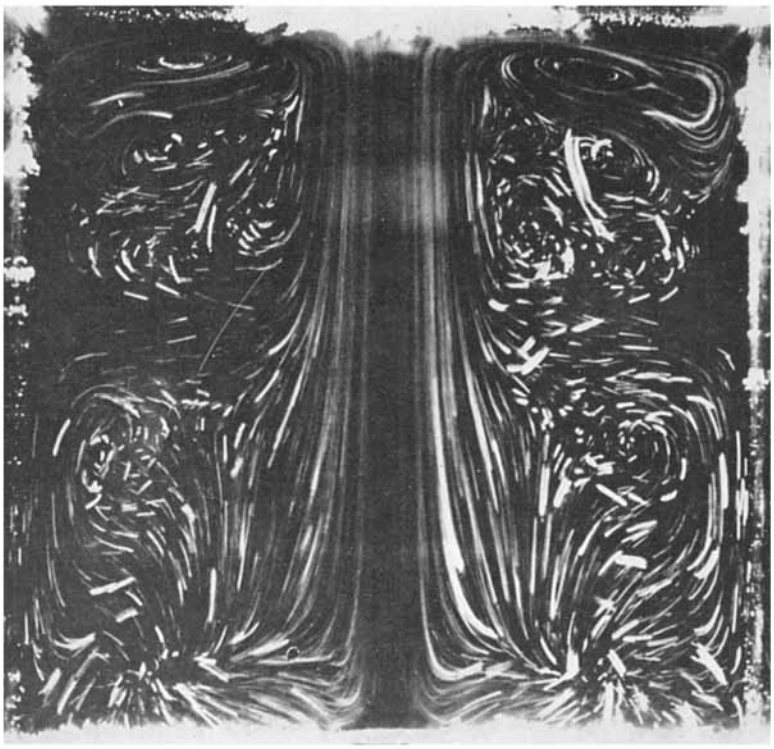

(*b*)

FIGURE 3. Effect of varying the Grashof number (Gr) in the rectangular enclosure. Illumination through the centre of the heated disk parallel to the shorter walls. (*a*) $Gr = 3 \times 10^7$; (*b*) $Gr = 1{\cdot}4 \times 10^8$.

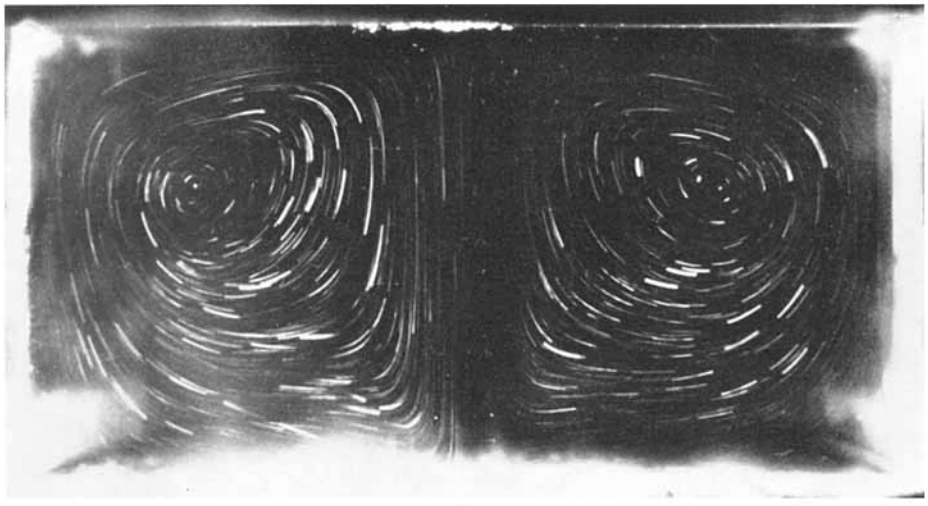

(*a*)

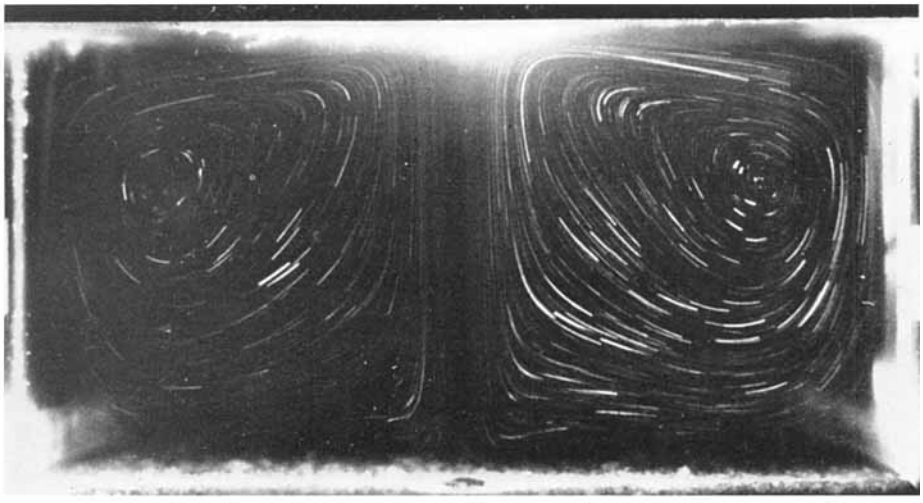

(*b*)

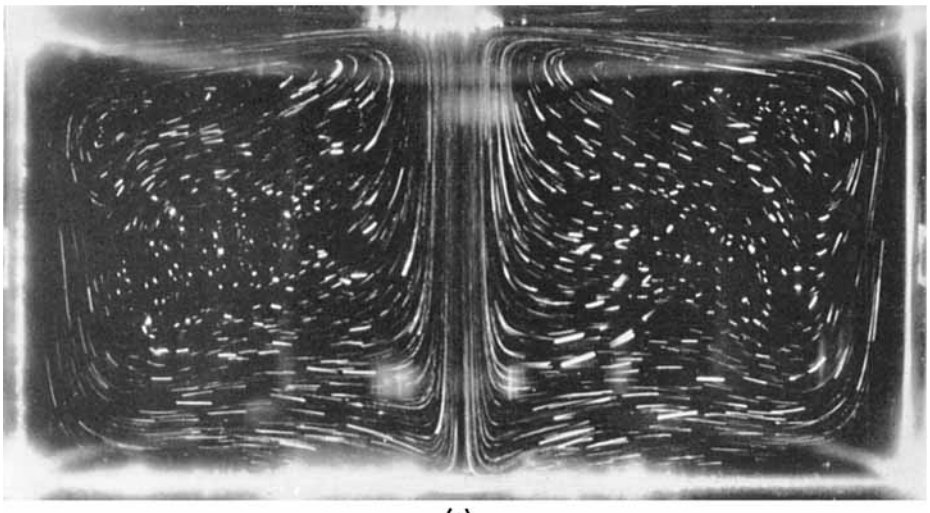

(*c*)

FIGURE 4(*a*), (*b*), (*c*). For legend see plate 4.

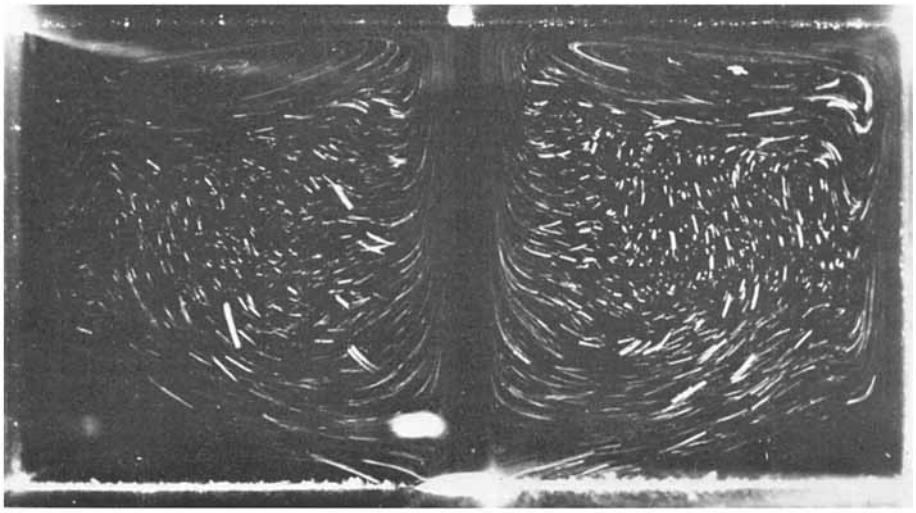

(*d*)

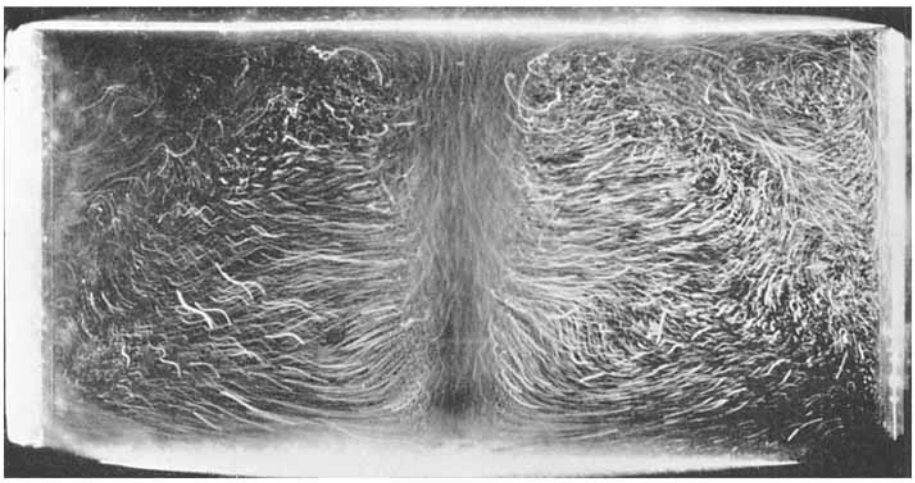

(*e*)

FIGURE 4. Effect of varying the Grashof number (Gr) in the circular chambers. Illumination through the centre of the heated disk. (*a*) $Gr = 8 \times 10^5$; (*b*) $Gr = 4 \times 10^6$; (*c*) $Gr = 4 \times 10^7$; (*d*) $Gr = 3 \times 10^8$; (*e*) $Gr = 1 \times 10^{10}$.

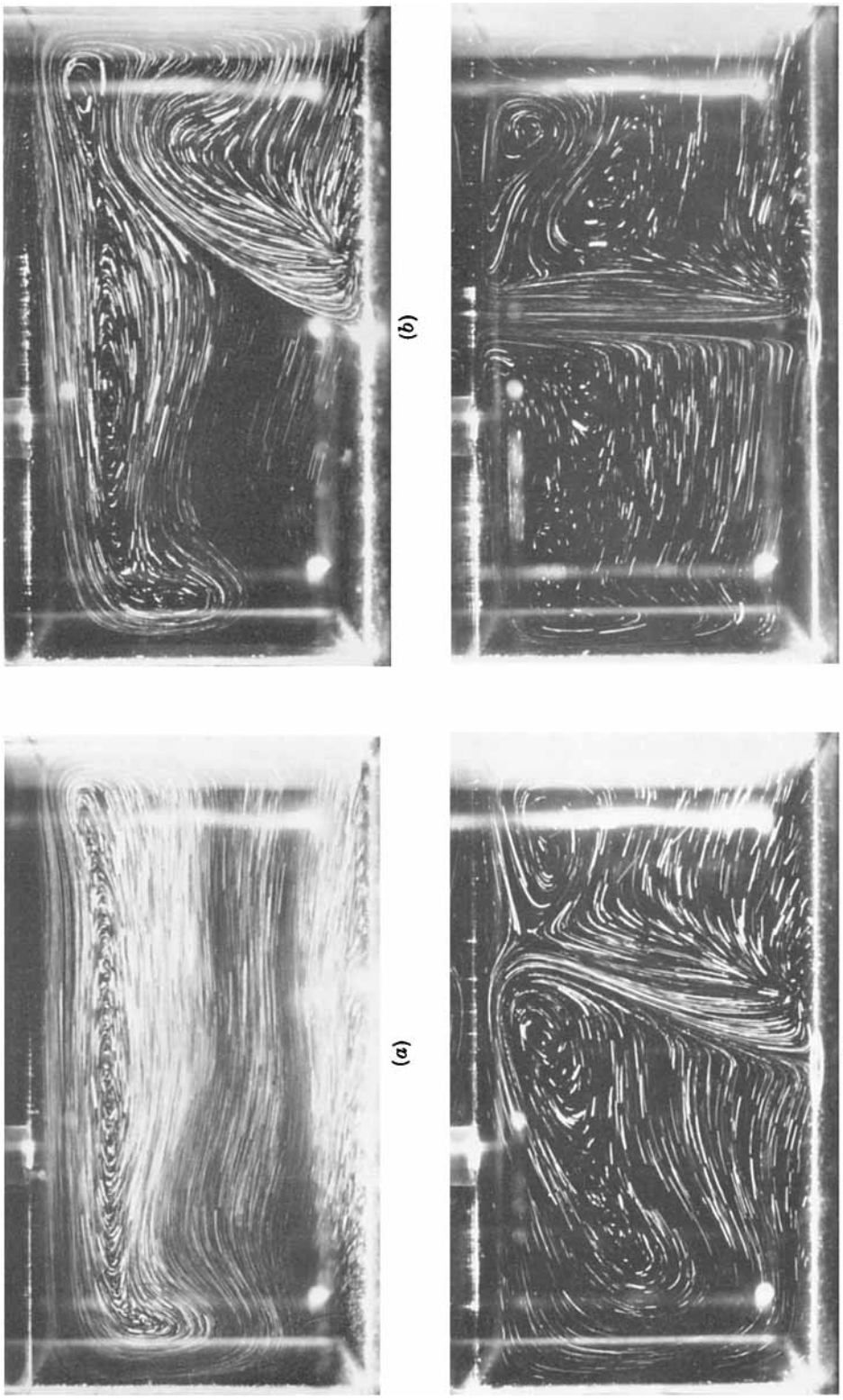

FIGURE 5. Effect of varying the Grashof number (Gr, based on heated-disk temperature) on the flow in a rectangular chamber with a heated right end wall. Illumination through centre of disk parallel to the longer walls. (*a*) $Gr = 0$; (*b*) $Gr = 4 \times 10^6$; (*c*) $Gr = 1 \times 10^7$; (*d*) $Gr = 1{\cdot}5 \times 10^8$.